

**Selective transformations between nanoparticle superlattices  
via the reprogramming of DNA-mediated interactions**

Yugang Zhang<sup>\*</sup>, Suchetan Pal<sup>\*†</sup>, Babji Srinivasan<sup>‡</sup>, Thi Vo<sup>†</sup>, Sanat Kumar<sup>†</sup>, and Oleg Gang<sup>\*#</sup>

<sup>\*</sup>*Center for Functional Nanomaterials, Brookhaven National Laboratory, Upton, NY, 11973*

<sup>‡</sup>*Department of Chemical Engineering, Indian Institute of Technology Gandhinagar,  
Ahmedabad, India 682525*

<sup>†</sup>*Department of Chemical Engineering, Columbia University, New York, NY 10027*

<sup>#</sup>*ogang@bnl.gov*

**The rapid development of self-assembly approaches has enabled the creation of materials with desired organization of nanoscale components. However, achieving dynamic control, wherein the system can be transformed on demand into multiple entirely different states, is typically absent in atomic and molecular systems and has remained elusive in designed nanoparticle systems. Here, we demonstrate with in situ small-angle x-ray scattering that, by using DNA strands as inputs, the structure of a three-dimensional lattice of DNA-coated nanoparticles can be switched from an initial 'mother' phase into one of multiple 'daughter' phases. The introduction of different types of re-programming DNA strands modifies the DNA shells of the nanoparticles within the superlattice, thereby shifting interparticle interactions to drive the transformation into a particular daughter phase. Moreover, we mapped quantitatively with free-energy calculations the selective re-programming of interactions onto the observed daughter phases.**

The creation of systems with adaptable and switchable structures is invaluable for achieving dynamic control of material functionality. Systems built from nanoparticles (NPs) often exhibit synergetic and collective properties; thus, regulated transformation of their large-scale organizations could offer a means of switching material properties. Several self-assembly methods, using the particles' sizes<sup>1</sup>, charges<sup>2</sup>, shapes<sup>3</sup>, packing effects<sup>4</sup>, polymerization-like growth<sup>5</sup>, field-induced assembly<sup>6</sup> and bio-recognition interactions<sup>7, 8, 9</sup>, have been demonstrated for the creation of NP superlattices, the structural basis of designed nanomaterials. If the interparticle molecular linkages are responsive, environmental factors, such as ionic strength<sup>10</sup>, pressure<sup>11</sup>, or pH<sup>12</sup>, can affect molecular conformations<sup>13</sup>, inducing, for instance, a change in interparticle distances. DNA-based approaches, being a powerful strategy for nanomaterial assembly<sup>7, 8, 14, 15</sup>, allow altering the state of interparticle DNA linkages in highly specific ways. For example, the ability to regulate DNA compact/extended states allows the fabrication of core-satellite nanoparticle clusters with changeable interparticle distances<sup>16</sup> and superlattices with switchable lattice constants<sup>17</sup>. However, it is significantly more challenging to control lattice transitions between different phases, crystallographic symmetries or morphological states, wherein global structural re-organization is required. One tentative example is to exploit peculiar temperature-dependent interactions, such as re-entrant liquid-solid-liquid transitions, as recently studied theoretically<sup>18, 19</sup> and experimentally<sup>20, 21</sup>.

Conceptually, it is exciting to imagine dynamically switchable systems, where a specific structure and the corresponding pathway can be chosen from multiple possible well-defined states and triggered as desired. Control of system transformations is crucial for creating materials whose functions can be activated on demand. To induce a structural change on a global scale, one requires a significant modification of either particle shape or particle interactions. For example, particle 'shape-shifting' was demonstrated as a means to induce structural transitions<sup>22, 23</sup>. However, the experimental realization of phase transformations via interaction- or shape-shifting is quite challenging due to the difficulty of creating suitable and tunable systems permitting crystal-to-crystal transitions, while insuring viable kinetic pathways. Here, we demonstrated a novel route for controlling transformations of DNA-NP superlattices into multiple phases via a post-assembly modification of the DNA shells; that is, re-programming of

interparticle interactions. By introducing different types of re-programming DNA strands, we selectively shift the particle-particle interactions, either by increasing both attraction and repulsion, or by separately increasing only attraction or only repulsion. These re-programmed interactions impose new constraints on particles. Consequently, the lattice can satisfy these constraints only by undergoing a transformation from the original ‘mother’ phase into one of the ‘daughter’ states, with the specific end state defined by the re-programmed interactions. Our experiments show that such selective transformations are fully controlled by the type of input DNA strand; thus, the system’s global crystalline structure can be switched on demand via these specific inputs. Using in-situ measurements, we observed a series of transitions from a *CsCl* phase to various phases, including *CuAu*, *HCP*, *quasi-2D*, *FCC*, and a *cluster* morphology. Moreover, we found that certain daughter phases, such as *HCP* and *quasi-2D*, required a mother-daughter pathway and could not be directly assembled from the solution of free NPs and the corresponding strands.

### **Experimental design and in-situ structural probing**

Our initial system (‘mother phase’) is built from ~10 nm gold nanoparticles (Au NPs) in a three-step process. First, the Au NPs were functionalized with single strand (ss) DNA (proto-DNA, Table S1) into proto-state NPs (Figure 1a). Second, the proto-state NPs were used to create a pair of complementary *X* and *Y* NPs (Figure 1b), which are able to hybridize with *x* and *y* base-DNA (in analogy to the common chromosome notation). Third, the *X* and *Y* NPs were assembled by mixing and subsequently crystalized into a ‘mother phase’, *MP*, (Figure 1c) by annealing at ~31°C (the melting temperature,  $T_m \sim 36^\circ\text{C}$ ). (See ‘Methods’ for details.)

We employed synchrotron-based small-angle x-ray scattering (SAXS) for in-situ probing of NP assemblies. The mother phase exhibits (Figure 2a, bottom) sharp rings in the 2D SAXS pattern; the corresponding structure factor  $S(q)$  (blue curve) can be indexed as a well-ordered body-centered cubic (*BCC*) lattice (see Supplementary Material ‘SAXS modeling’ for details, Figure S8). The so-formed mother phase is stable over at least several months (Figure S13). However, by introducing the re-programming strands, we modify the DNA shells of NPs in the mother phase, which shifts the inter-shell interactions, resulting in a lattice transformation, as we discuss below.

## Selective lattice transformations by modifying DNA shell

First, we discuss the concept of a dynamically tunable NP shell for programmable phase-transformations in the context of DNA-NP assemblies. In contrast to free DNA strands, the interactions of which are mainly governed by sequence-determined Watson-Crick base-pairing, the interactions of DNA-coated particles depend on the composition of DNA shells<sup>24, 25, 26, 27</sup>. We propose to modulate NP shells in a dynamical fashion when particles are already inter-connected in the assembled lattice, by providing different types of input strands that are able to become an integral part of the shell. Depending on the connectivity properties of these inserted strands, shell interactions can be manipulated in desired ways. This re-programming of interactions can trigger structure transformations.

We hypothesize that the DNA chain configurations on the surface of a free NP are distinct from those between particles in the assembled lattice. For a free un-assembled NP, not all proto-strands on the NP surface are able to hybridize with  $x$  and  $y$  base-DNA depending on concentration. Indeed, crowding of single-stranded  $x$  and  $y$  base-DNA on the NP can partially block the proto-DNA sites, as illustrated in Figure 1b; there is also an entropy loss for base-DNAs attached to the NP in comparison to their solution state. In contrast, when NPs are assembled in a condensed phase, the proto-DNA sites could be unblocked: the formation of double helix bonds between NPs reduces chain entropy and affects local DNA conformations (see Figure 1c). These now-opened sites can host the new input strands, which have one end complementary to proto-DNA, while the other end can provide different custom interaction-shifting functions, as we show below. We stress that the only requirement is that certain hybridization/non-hybridization rules should be satisfied; this interaction re-programming approach does not rely on the use of particular DNA sequences.

To test our hypothesis, we measured the number of proto- ( $N_p$ ) and base-DNA ( $N_x$  or  $N_y$ ) on the surface of free particles, as well as the number of available DNA sites in the assemblies ( $N_{open}$ ). Using a modified reported procedure<sup>28</sup>, we found that  $N_p$ ,  $N_x$ , and  $N_{open}$ , respectively, were  $\sim 50$ ,  $34$ , and  $8$  (see supporting material, ‘DNA number quantification’). Thus, the transition from free NPs to their condensed (aggregated) state, in which DNAs between NPs are

hybridized, unblocks about 20-25% of previously unavailable of proto-sites. These sites are used in our study for in-situ modifications of DNA shells with re-programming strands. Our study on the kinetics of input strand incorporation within the lattices demonstrated that strand diffusion and hybridization required 2-3 hours (Figure S4), which was significantly shorter than our typical incubation time, about 24 hours, at room temperature ( $RT \sim 23^\circ\text{C}$ ).

We explored three types of input re-programming strands, all of which exerted distinct additional effects on the inter-particle interactions: ‘blending’, ‘stapling’, and ‘repelling’, as shown in Figure 1. The three types of modifications accordingly provide the following interactions: (i) a mixed attraction and repulsion between all particles types (‘blending’) instead of repulsion-only and attraction-only as in the mother phase, (ii) dominated inter-particle attraction (‘stapling’), and, (iii) predominant repulsion between neighboring particles (‘repelling’). Although the interaction-shifting does not depend on specific sequences, as long as input DNA strands fulfill their designated roles, the magnitude of the interaction-shift may depend on the DNA length<sup>29, 30</sup>, melting temperature, and the inert DNA tails<sup>31</sup>.

Experimentally, for the ‘blending’ case, we added an equal mixture of  $x$  and  $y$  DNA strands ( $x$  &  $y$ ) to the solution with the assembled aggregate, and these strands altered the shells of  $X$  and  $Y$  NPs. As such, both the  $x$  and  $y$  strands can hybridize randomly with the now unblocked proto-DNA on the surface of the  $X$  and  $Y$  particles (Figure 1d), which allows adding  $x$  onto  $Y$  NP and  $y$  onto  $X$ . This ‘blending’ results in additional attraction, as well as repulsion, between  $X(Y)$  and  $X(Y)$ <sup>27</sup>. For the ‘stapling’ case, the input DNA ( $s$ ) is designed with both ends complementary to proto-DNA. This design thus increases attraction between next-neighbor NPs, regardless of the particle type (Figure 1e). Note that the polarity of hybridization of stapling strands with base-DNAs requires folding of stapling linkages (see Figure S5). Finally, ‘repelling’ ( $r$ ) DNAs, whose two ends are respectively complementary and non-complementary to proto-DNA, generate additional repulsion between all next-neighbor particles<sup>24</sup> (Figure 1f).

Due to the input of the new types of strands, and some free sites available for DNA hybridization on a particle’s surface, a certain amounts of these newly added re-programming strands will be incorporated into the DNA shells of the NPs. We thus denote the shell-modified  $X$  and  $Y$  particles as  $X_y$  and  $Y_x$ ,  $X_s$  and  $Y_s$ , and  $X_r$  and  $Y_r$ , respectively, for ‘blending’, ‘stapling’, and

‘repelling’ input strands. Such targeted-shell modifications can result in phase transformations, as we revealed below. Considering these interaction types, we denote the above three resulting phases respectively as daughter phase blending ( $DP\_B$ ), stapling ( $DP\_S$ ), and repelling ( $DP\_R$ ).

### Phase transformation by blending strands

The particle types in the ‘mother’ phase interact in a well-defined manner: similar particles (XX or YY) repel, and different particles types (XY) attract. However, the input of blending strands modifies these interactions significantly; overall, attraction and repulsion now exist between similar and complementary particles respectively, as schematically shown by the red-blue interaction bar in Figure 1d. This new interaction scheme can be accommodated only if the superlattice transforms into a different structure. Using in-situ SAXS measurements, we monitored the transformation in real-time, when the system was brought to about 28°C. Remarkably, we observed (Figure 2) the ‘birth’ of a new  $DP\_B$  phase ( $T_m \sim 37^\circ\text{C}$ ), the gradual appearance of which was accompanied by the fading of the mother  $BCC$  phase (the modeling is shown in Fig. S8), as revealed from the  $S(q)$  time-evolution (Figure 2b). The daughter structure shows sharp rings in the 2D pattern (Figure 2a top). The obtained  $S(q)$  (Figure 2b, red curve,) indicates that  $DP\_B$  is a well-ordered face-centered cubic ( $FCC$ ) lattice (see Figure S9 for structure modeling). During the  $BCC$  to  $FCC$  transition, the position ( $q_1$ ) of the first peak in  $S(q)$  remains practically unchanged. This implies that the first nearest-neighbor center-to-center interparticle distance ( $D_{cc}$ ) is preserved (Figure 2c), given the same factor for the position of  $q_1$ ,  $D_{cc} = \sqrt{6} \cdot \pi / q_1$ , for the  $BCC$  (diffraction peak 100) and  $FCC$  (diffraction peak 111) lattices. Figure 2c depicts the emergence of the daughter phase, whose volume fraction,  $\phi$  (red open squares), gradually increases, as revealed by our SAXS analysis. By fitting the  $S(q)$  with a model that accounts for both  $BCC$  and  $FCC$  phases (see supporting material and Figures S11(a-j)), we obtained the time evolution of  $\phi$ . No intermediate phase was observed during this transformation, as indicated by the fits. Such a first-order solid-solid diffusionless transformation from  $BCC$  to  $FCC$  has been observed for atomic-<sup>32</sup> and polymeric-systems<sup>33</sup> under a thermal field. A recent study also suggested similar transition for DNA-coated submicron particles<sup>27</sup>, although the transformation was not controlled and the pathway has not been revealed.

Our measurements allow quantifying the transformation pathway by establishing the relationship between the structural correlation length ( $\xi$ , a measure of structural order) and the Williamson Hall slope ( $\varepsilon$ , a relative measure of strain-induced average lattice distortion)<sup>34</sup> with the development of the *DP\_B* (*FCC*) phase using the data fits (Figures S11(a-j)). Figure 2d demonstrates that  $\varepsilon$  first increases  $\sim 5$  times until  $\phi \sim 0.6$ , and then gradually decreases to the initial level of *DP\_B*. This behavior is possibly caused by the nucleation and growth of *FCC* ‘embryos’; i.e. strain develops as domains of the new phase form and expand in a matrix of the mother-phase. In contrast,  $\xi$  monotonically decreases from  $\sim 340$  nm in the original *BCC*, to  $\sim 200$  nm in the *FCC*, which indicates a modest reduction of grain size.

### Compositional order and phase-transformation

One of the important characteristics of binary lattices is its compositional order; i.e., the degree of particles occupying the ‘correct’ sites. For example, according to previous studies<sup>8, 30 7, 35</sup>, the *MP*, comprising two types of particles distinguished by their DNA shells, should form a *CsCl*-type compositional ordered phase. Recently, it was also shown that the degree of compositional order of *CsCl*-type NP superlattices was progressively reduced for larger single-stranded DNA shells<sup>30</sup>. It is intriguing to explore how such solid-solid transformation affects the compositional order. Indeed, the binary *DP\_B* could present a compositional disordered *FCC*, or an ordered *CuAu*-type lattice.

To examine the compositional order, distinct particle ‘colors’ (different ability to scatter x-rays) are required. To probe this aspect, we investigated a system consisting of two components with distinctively different x-ray scattering properties; namely, 10 nm Au NPs, and  $\sim 6.5$  nm CdSe/Te@ZnS quantum dots (QDs) with proto-DNA  $\sim 30$ -40 (see Figure S6 and S7 for SEM images). Following the same protocol as for Au-Au systems, we assembled Au and QD into *MP* (*Au-QD MP*). The obtained  $S(q)$  and the structures are shown in middle panels of Figure S14a-b. We note a lower degree of crystallinity for Au-QD system (vs Au-Au), which might arise from the lower number of tethered strands, as well as the somewhat ellipsoidal shape and larger size distribution of QD<sup>30</sup>.

We first confirmed, by modeling of  $S(q)$ , that mother phase exhibited compositional order (Figure S14a-b, middle panel). We then verified, using UV-vis measurements, that no particles were released from the assemblies to the supernatant during the transformation; thus, we concluded that  $DP\_B$  possesses the same stoichiometry of particles  $X$  and  $Y$  as in the mother lattice. Consistent with the Au-Au system, the  $MP$  of the  $Au-QD$  system remained unchanged upon temperature annealing if no blending strands ( $x$  &  $y$ ) are added (Figure S14a-b bottom panel). However,  $Au-QD$   $MP$  was transformed into a new phase (Figure S14a-b top panel), as indicated by the change of relative positions of the first- and second-peaks ( $q_1$  and  $q_2$ , respectively), upon input of  $x$  &  $y$  strands. Despite the weaker structural order, the value of  $q_2/q_1$  clearly changes from  $\sqrt{2}$  (the dashed line in Figure S8b) in  $MP$ , to  $\sqrt{3}$  in  $DP\_B$ . The first two peaks are indexed as the (100) and (110) in  $BCC$ -type, and as (100) and (111) in  $FCC$ -type lattices. The existence of the (100) peaks indicates good compositional order<sup>30</sup> in both structures, implying the formation of  $CsCl$  and  $CuAu$  lattices (Figure S14). A further structural simulation<sup>36</sup>, shown as a solid line in Figure S14a, agrees well with the experimental spectra, using the proposed  $CsCl$ - and  $CuAu$ -structural models for the corresponding systems.

### Polymorphism for transformations by stapling strands

We next investigated the structural transformation of mother phase ( $BCC$ , as shown in Figure 3a) to stapling ( $DP\_S$ ) state upon introducing re-programming strands that increased interparticle attraction regardless of particle types (Figure 1e). The details of duplex formation are given in Table S3 and depicted in Figure S5. In contrast to the transition induced by blending strands, the  $DP\_S$  phase does depend on annealing temperature. Figure 3d shows the 2D SAXS pattern and the corresponding  $S(q)$  of the new daughter stapling phase. We observed transformation at a higher temperature ( $\sim 34^\circ\text{C}$ ,  $T_m$  of  $DP\_S \sim 39^\circ\text{C}$ ) into an  $FCC$  lattice, denoted as  $DP\_S_{HT}$  (Fig. 3 b,c) However, a different phase, denoted as  $DP\_S_{LT}$ , was found when the transformation occurred at lower temperature ( $\sim 28^\circ\text{C}$ ). In this case, a hexagonal close-packed ( $HCP$ ) structure emerged, as confirmed by the indexing and modeling (Figure 3d and Figure S10). Interestingly, the newly-formed  $HCP$  phase shows grain sizes about 4-5 times larger than the mother phase. Additionally, the scattering pattern displays strip-like features (pointed out by the blue arrows in the top panel in Figure 3b inset); they indicate the presence of  $2D$ -like crystals in the  $HCP$  phase. Due to a lower temperature of formation, the  $HCP$  phase is a kinetically

metastable state, as was verified by the further transformation into an *FCC* phase during annealing at  $\sim 32^\circ\text{C}$ . Previous simulation work on hard-sphere systems demonstrated a transition from *HCP* to *FCC* by the removal of stacking faults as crystals grew larger<sup>37</sup>. The kinetic nature of the observed *HCP* also agrees with theoretical considerations<sup>38, 39</sup> and previous experimental observations<sup>35, 40</sup>. Moreover, we obtained similar results for systems with stronger coupling (19-base) between stapling and base-DNA strands vs. 14-base in the discussed *DP<sub>S</sub>* system. Interestingly, the system exhibits a phase polymorphism for this transition: both the *DP<sub>SLT</sub>* and *DP<sub>HT</sub>* phases could only be obtained via the transformation pathway from the *MP*. These phases could not be assembled from free particles and the corresponding DNAs; namely, proto-state particles mixed with *x*, *y*, *s* strands did not even form an aggregate (Figure S15).

The transition from the *BCC* to the *FCC* and *HCP* phases for stapling scenarios can be understood qualitatively by considering the involved interactions. The stapling strands, by connecting particles irrespective of their types and, thus, increasing interparticle attraction, play a similar role to self-complementary DNA shells, which result in *FCC* structures as reported<sup>7</sup>. From the viewpoint of crystal structure, the *FCC*- and *HCP*-lattices represent different stacking sequences of hexagonally close-packed layers, *AB-AB* for *HCP* and *ABC-ABC* for *FCC* (Figure 3c and e). Due to the negligible inter-particle enthalpy difference, and only slightly different entropy<sup>38</sup>, it is plausible that a kinetic product, *HCP*, is formed instead of the *FCC* phase. Additionally, in our DNA design, the stapling strand (30 bases) is much shorter than the combined length base-DNAs (58 bases, see Fig S5 for the hybridization scheme), but the hybridization energy between stapling strands and proto-DNA is larger than between the *x* and *y* base-DNAs. Therefore, due to the imposed stress, some bonds between base-DNAs might open when *s*-DNA is hybridized. Since binding between hexagonal layers is weaker than that within a layer (smaller particle-coordination number), some uncorrelated stacking of layers can occur. Recent computational work predicted the formation of a random *HCP* (*RHCP*) structure<sup>41</sup> that was not previously observed. In the extreme case of a full decoupling between layers, and a complete loss of their structural correlation, 2D nanoparticle arrays may be formed; this scenario is possible, given our observations.

### **Repelling strands-induced transition to cluster morphology**

Finally, we examined the structural reconfiguration induced by a room-temperature incorporation of repelling,  $r$ , strands into the  $MP$  lattice; such  $r$ -strands add a steric interparticle repulsion (Figure 1f). We brought the modified system to different temperatures to allow for the transformation, and then reduced it back to  $RT$  and performed SAXS. Upon incorporation of  $r$ -strands at  $RT$ , we observed only a moderate change of  $S(q)$ , indicating somewhat reduced correlation length of the preserved BCC lattice. This behavior occurred below a transition temperature of about 34°C, as shown in Figure 4a (see Figure S16 for details). However, a significant broadening of scattering peaks happened for temperatures  $> 34^\circ\text{C}$  (Figure 4a), and persisted even after the sample was cooled to  $RT$ . This  $S(q)$  change was accompanied by a morphological transition from a condensed aggregate to a suspended phase ( $DP\_R$ ), as apparent from the color change of the supernatant (photographs Fig. 4b).

We characterized the suspended morphology using dynamic light scattering (DLS), and by modeling the scattering profile (Figure 4a, red data), as shown in Figure S12. DLS indicates that the suspension consists of clusters with sizes on the order of hundreds of nm (around 200 particles per cluster) with a broad size distribution (Figure 4b inset and Figure S17). We compare the temperature dependence of the correlation length  $\xi(T)$  in Figure 4b with DLS results and macroscopic observations. When  $r$  strands are added, an abrupt  $\xi$  decrease occurs, from about 300 nm to 90 nm, at the transition temperature. We propose that the incorporation of  $r$ -strands in a shell imposes only internal pressure due to steric effects, but the lattice remains intact because of  $x$ - $y$  linkages between NP shells. However, close to the transition temperature those interparticle bridges (between  $x$  base- and  $y$  base-DNAs linkages) start to partially melt; consequently, lattice order is decreased. When the temperature is reduced back to  $RT$ , particles cannot form a continuous phase due to the steric repulsion of  $r$ -strands. Instead, a cluster state is formed as a compromise to satisfy some  $x$ - $y$  hybridizations.  $S(q)$  reveals (Figure 4) a similar position ( $q_1$ ) of the first scattering peak for mother  $BCC$  and daughter cluster morphology. Since the interparticle distances for those two cases are determined by a similar pre-factor, i.e.  $D_{cc} = \sqrt{6} \times \pi / q_1$  for  $BCC$  and  $D_{cc} = 2.45 \times \pi / q_1$ <sup>42</sup> for unstructured cluster, we conclude that the transition does not affect interparticle distances. The repelling interaction, due to its steric nature, can be further modulated by changing the length of  $r$  strands. For example, we found that in order to

induce such a *BCC-to-cluster* transition, longer (30-base) tails were required; a short tail (20-base) resulted only in a subtle structural change of the mother *BCC* lattice.

### **Modeling of input strands-induced interaction-shifting**

We further established a quantitative relationship between the different types of input re-programming strands, and the modification of inter-particle interactions that led to the observed transformations. Our calculations were carried out in three steps; namely, interactions parameterization, pair-interactions modeling, and lattice free-energy calculation (see supporting information ‘interparticle interactions’ part, Figure S18-19 and Table S3, for details of the calculation). First, we parameterized our DNA shell components using a shell modification factor ( $\gamma$ ), which was defined as a number ratio of strands that were different-to-particle (e.g.,  $x$  to  $Y$ ) to strands that were same-to-particle (e.g.  $x$  to  $X$ ). For instance, one computes  $\gamma = 0$  for a shell with one component and  $\gamma \sim 0.24$  ( $= 8/34$ ) for the repelling case. Thus, a larger  $\gamma$  indicates a higher degree of shell modification. The  $\gamma$ -dependent DNA shells in systems *DP\_B*, *DP\_S* and *DP\_R* accordingly are depicted in Figure 5 (a-c), where the corresponding  $\gamma$  is estimated from the experimental data as  $\sim 0.11$ ,  $0.24$ , and  $0.24$ , respectively. Second, we developed a DNA-shell interaction model for a two-particle system, and calculated the free energy based on the derived canonical partition function. Third, the free energy of a lattice unit cell was calculated as a function of structure symmetry and lattice parameters.

The calculation results for pathways from mother phase to different daughter phases (*DP\_B*, *DP\_S*, and *DP\_R*) are shown in Fig 5 (a-c). Since our *BCC* is actually a binary-lattice with respect to surface-attached DNA, namely a *CsCl* lattice, we calculated the energy for *CsCl* rather than that of mono-component *BCC*. In the case of for blending daughter phase (*DP\_B*), the *AuCu* lattice becomes energetically favorable over *CsCl* when  $\gamma > \sim 0.1$ , which is comparable with the experimental value of  $\gamma \approx 0.11$ , and, thus, explains the stable *AuCu* phase (Figure 2,3 and Figure 5d top left). The calculation for stapling daughter phase (*DP\_S*) reveals that *FCC* and *HCP* are energetically indistinguishable in our model; however, the hydrodynamic correlation

movements between particles<sup>41</sup> might play a role in the observed formation of temperature-dependent phases. Nevertheless, the results show that both phases are more favorable than *CsCl* at  $\gamma > \sim 0.14$ . Hence, our experimental  $\gamma \approx 0.24$  supports the dominance of the *FCC* or *HCP* over the *CsCl* phase. As for the repelling daughter phase (*DP<sub>R</sub>*), our model shows that repulsion energy ( $F_r$ ) exceeds attraction energy ( $F_a$ ) at  $\gamma \approx 0.3$ , and, therefore, the assemblies will dissociate upon such shell modification. For our experimental case, the modification of DNA shells by  $r$  strands results in  $|F_r/F_a| \sim 0.7$  and  $\gamma \approx 0.24$ , which are indicative of lattice destabilization, and a transition to a cluster morphology (Figures 4 and 5d bottom left).

In summary, we have demonstrated the selective transformations of DNA-nanoparticle superlattices into distinctive structures by introducing specific types of strands that modify interparticle interactions within the lattice. We have related quantitatively the DNA-induced interaction-shifting and the resultant phases. The demonstrated dynamic switching of the entire superlattice will allow creating reprogrammable and switchable materials, wherein multiple states can be activated for enabling different functional properties. Furthermore, the common susceptibility to the genetic input of the nanoparticle-based materials discussed herein and of living matter might open intriguing routes for dynamical interfacing between biological and manmade systems. The presented concept might also open possibilities for “genetic engineering” of DNA-based nanoscale materials.

## Methods

**Assembly of DNA functionalized gold nanoparticles into ‘mother phase’.** Our initial system (‘mother phase’) is built from  $\sim 10$  nm gold nanoparticles (Au NPs) in a three-step process. First, we synthesized the building blocks (Au NPs), and attached 30-base single strand (ss) DNA<sup>8</sup> (Table S1) to their surfaces; these are correspondingly denoted as proto-state NPs (Figure 1a) and proto-DNA. Second, we generated base-NP by hybridizing proto-NP with base-DNA (Figure 1b). The proto-state NPs (in 140 mM NaCl phosphate buffer) were split into two portions, and correspondingly hybridized (Figure 1b) with the  $x$  and  $y$  base-DNA (in analogy to the common chromosome notation) to produce  $X$  and  $Y$  NP. The  $x$ - and  $y$ - strands contain the same 20-base sequence at their ends, which are complementary to the NP-tethered proto-DNA, while the other 8-base ends of  $x$  and  $y$  are mutually complementary. After purifying the excess

DNA, we obtained a set of complementary particles ( $X$  and  $Y$ ), denoted as base-state NPs (hydrodynamic radius  $R_e \sim 18$  nm, Figure S17). Third, we assembled the mother system by combining equivalent amounts of complementary particles  $X$  and  $Y$ . The assembly was crystalized further into a mother phase,  $MP$ , (Figure 1c) by annealing at  $\sim 31^\circ\text{C}$  (the melting temperature,  $T_m \sim 36^\circ\text{C}$ ).

**Phase transformations of ‘mother phase’ by using DNA strands as input.** Different types of DNA strands were introduced into the solution with the assembled ‘mother phase’. The in-situ structure evolution as a function of temperature and time were monitored. (See Main text ‘Selective lattice transformations’ for details.)

**Characterization of nanoparticles and assemblies.** The morphology of nanoparticles was characterized by electron microscopy. The number of proto-DNA, base-DNA and the incorporated input-DNA were determined based on the reported fluorescence-based method. Synchrotron-based SAXS (NSLS X-9) was employed to probe the *in-situ* structure of particles assemblies. (See Supplementary Information ‘Methods’ and ‘DNA number quantification’ for details.)

**Modelling of SAXS profiles and interparticle interactions.** To simulate powder SAXS profiles, based on our previous work<sup>30, 36</sup>, we developed a scattering formalism, which accounted for particle size, polydispersity, lattice disorder and micro-strain, average grain size, for single-phase, binary phase, and cluster systems. For a quantitative understanding of the input-DNA induced phase transformations, we developed a pairwise DNA-shell interaction model based on the reported<sup>26, 35</sup> and calculated the free energy between a pair of particles, and then calculated the free energy in different crystal structures. (See Supplementary Information ‘SAXS’ and ‘Calculation of interparticle interactions’ for details.)

## Acknowledgements

We thank Dr. Kevin Yager, Prof. Venkat Venkatasubramanian, and Dr. Lijun Wu for helpful discussions. We thank Dr. Fang Lu for help with DLS and DNA hybridization kinetics measurements. Research carried out at the Center for Functional Nanomaterials and National

Synchrotron Light Source, Brookhaven National Laboratory, is supported by the U.S. Department of Energy, Office of Basic Energy Sciences, under Contract No. DE-SC0012704. Research at Columbia University was supported by the US Department of Energy, Office of Basic Energy Sciences, Division of Materials Sciences and Engineering under Award DE-FG02-12ER46909.

### **Author Contributions**

Y.G.Z and O.G. conceived the concept and designed experiments. Y.G.Z. performed the experiments and analysed the data, S. P. contributed to the measurements, O.G. contributed to the data analysis. Y.G.Z., B.S., T.V., and S.K. contributed to modelling of particle interactions Y.G.Z. and O.G. wrote the paper. O.G. supervised the project. All authors discussed the results and commented on the manuscript.

### **Additional information**

Correspondence and requests for materials should be addressed to O.G.

### **Competing financial interests**

The authors declare no competing financial interests.

### **References**

1. Redl FX, Cho KS, Murray CB, O'Brien S. Three-dimensional binary superlattices of magnetic nanocrystals and semiconductor quantum dots. *Nature* 2003, **423**(6943): 968-971.
2. Kostiainen MA, Hiekkataipale P, Laiho A, Lemieux V, Seitsonen J, Ruokolainen J, *et al.* Electrostatic assembly of binary nanoparticle superlattices using protein cages. *Nat Nanotechnol* 2013, **8**(1): 52-56.
3. Glotzer SC, Solomon MJ. Anisotropy of building blocks and their assembly into complex structures. *Nat Mater* 2007, **6**(8): 557-562.
4. Damasceno PF, Engel M, Glotzer SC. Predictive Self-Assembly of Polyhedra into Complex Structures. *Science* 2012, **337**(6093): 453-457.
5. Liu K, Nie ZH, Zhao NN, Li W, Rubinstein M, Kumacheva E. Step-Growth Polymerization of Inorganic Nanoparticles. *Science* 2010, **329**(5988): 197-200.

6. Yan J, Bloom M, Bae SC, Luitjen E, Granick S. Linking synchronization to self-assembly using magnetic Janus colloids. *Nature* 2012, **491**(7425): 578-581.
7. Park SY, Lytton-Jean AKR, Lee B, Weigand S, Schatz GC, Mirkin CA. DNA-programmable nanoparticle crystallization. *Nature* 2008, **451**(7178): 553-556.
8. Nykypanchuk D, Maye MM, van der Lelie D, Gang O. DNA-guided crystallization of colloidal nanoparticles. *Nature* 2008, **451**(7178): 549-552.
9. Geerts N, Eiser E. DNA-functionalized colloids: Physical properties and applications. *Soft Matter* 2010, **6**(19): 4647-4660.
10. Xiong HM, Sfeir MY, Gang O. Assembly, Structure and Optical Response of Three-Dimensional Dynamically Tunable Multicomponent Superlattices. *Nano Lett* 2010, **10**(11): 4456-4462.
11. Srivastava S, Nykypanchuk D, Maye MM, Tkachenko AV, Gang O. Super-compressible DNA nanoparticle lattices. *Soft Matter* 2013, **9**(44): 10452-10457.
12. Roiter Y, Minko I, Nykypanchuk D, Tokarev I, Minko S. Mechanism of nanoparticle actuation by responsive polymer brushes: from reconfigurable composite surfaces to plasmonic effects. *Nanoscale* 2012, **4**(1): 284-292.
13. Tokarev I, Minko S. Tunable plasmonic nanostructures from noble metal nanoparticles and stimuli-responsive polymers. *Soft Matter* 2012, **8**(22): 5980-5987.
14. Knorowski C, Burleigh S, Travesset A. Dynamics and Statics of DNA-Programmable Nanoparticle Self-Assembly and Crystallization. *Phys Rev Lett* 2011, **106**(21): 215501.
15. Halverson JD, Tkachenko AV. DNA-programmed mesoscopic architecture. *Phys Rev E* 2013, **87**(6): 062310.
16. Sebba DS, Mock JJ, Smith DR, LaBean TH, Lazarides AA. Reconfigurable core-satellite nanoassemblies as molecularly-driven plasmonic switches. *Nano Lett* 2008, **8**(7): 1803-1808.
17. Maye MM, Kumara MT, Nykypanchuk D, Sherman WB, Gang O. Switching binary states of nanoparticle superlattices and dimer clusters by DNA strands. *Nat Nanotechnol* 2010, **5**(2): 116-120.

18. Russo J, Tavares JM, Teixeira PIC, da Gama MMT, Sciortino F. Re-entrant phase behaviour of network fluids: A patchy particle model with temperature-dependent valence. *J Chem Phys* 2011, **135**(3): 034501.
19. Angioletti-Uberti S, Moggetti BM, Frenkel D. Re-entrant melting as a design principle for DNA-coated colloids. *Nat Mater* 2012, **11**(6): 518-522.
20. Feng L, Laderman B, Sacanna S, Chaikin P. Re-entrant solidification in polymer–colloid mixtures as a consequence of competing entropic and enthalpic attractions. *Nat Mater* 2015, **14**(1): 61-65.
21. Rogers WB, Manoharan VN. Programming colloidal phase transitions with DNA strand displacement. *Science* 2015, **347**(6222): 639-642.
22. Zhang YG, Lu F, van der Lelie D, Gang O. Continuous Phase Transformation in Nanocube Assemblies. *Phys Rev Lett* 2011, **107**(13): 135701.
23. Nguyen TD, Jankowski E, Glotzer SC. Self-Assembly and Reconfigurability of Shape-Shifting Particles. *Acs Nano* 2011, **5**(11): 8892-8903.
24. Maye MM, Nykypanchuk D, van der Lelie D, Gang O. DNA-Regulated micro- and nanoparticle assembly. *Small* 2007, **3**(10): 1678-1682.
25. Nykypanchuk D, Maye MM, van der Lelie D, Gang O. DNA-based approach for interparticle interaction control. *Langmuir* 2007, **23**(11): 6305-6314.
26. Dreyfus R, Leunissen ME, Sha RJ, Tkachenko AV, Seeman NC, Pine DJ, *et al.* Simple Quantitative Model for the Reversible Association of DNA Coated Colloids. *Phys Rev Lett* 2009, **102**(4): 048301.
27. Casey MT, Scarlett RT, Rogers WB, Jenkins I, Sinno T, Crocker JC. Driving diffusionless transformations in colloidal crystals using DNA handshaking. *Nat Commun* 2012, **3**(1209): 1.
28. Demers LM, Mirkin CA, Mucic RC, Reynolds RA, Letsinger RL, Elghanian R, *et al.* A fluorescence-based method for determining the surface coverage and hybridization efficiency of thiol-capped oligonucleotides bound to gold thin films and nanoparticles. *Anal Chem* 2000, **72**(22): 5535-5541.
29. Xiong HM, van der Lelie D, Gang O. Phase Behavior of Nanoparticles Assembled by DNA Linkers. *Phys Rev Lett* 2009, **102**(1): 015504.

30. Zhang YG, Lu F, Yager KG, van der Lelie D, Gang O. A general strategy for the DNA-mediated self-assembly of functional nanoparticles into heterogeneous systems. *Nat Nanotechnol* 2013, **8**(11): 865-872.
31. Di Michele L, Mognetti BM, Yanagishima T, Varilly P, Ruff Z, Frenkel D, *et al.* Effect of Inert Tails on the Thermodynamics of DNA Hybridization. *J Am Chem Soc* 2014, **136**(18): 6538-6541.
32. Sandoval L, Urbassek HM, Entel P. The Bain versus Nishiyama-Wassermann path in the martensitic transformation of Fe. *New J Phys* 2009, **11**: 103027.
33. Bang J, Lodge TP, Wang XH, Brinker KL, Burghardt WR. Thermoreversible, epitaxial fcc  $\leftrightarrow$  bcc transitions in block copolymer solutions. *Phys Rev Lett* 2002, **89**(21): 215505.
34. Williamson GK, Hall WH. X-Ray Line Broadening from Filed Aluminium and Wolfram. *Acta Metall Mater* 1953, **1**(1): 22-31.
35. Macfarlane RJ, Lee B, Jones MR, Harris N, Schatz GC, Mirkin CA. Nanoparticle Superlattice Engineering with DNA. *Science* 2011, **334**(6053): 204-208.
36. Yager KG, Zhang YG, Lu F, Gang O. Periodic lattices of arbitrary nano-objects: modeling and applications for self-assembled systems. *J Appl Crystallogr* 2014, **47**: 118-129.
37. Pronk S, Frenkel D. Can stacking faults in hard-sphere crystals anneal out spontaneously? *J Chem Phys* 1999, **110**(9): 4589-4592.
38. Woodcock LV. Entropy difference between the face-centred cubic and hexagonal close-packed crystal structures. *Nature* 1997, **385**(6612): 141-143.
39. Mau SC, Huse DA. Stacking entropy of hard-sphere crystals. *Phys Rev E* 1999, **59**(4): 4396-4401.
40. Hoogenboom JP, Derks D, Vergeer P, van Blaaderen A. Stacking faults in colloidal crystals grown by sedimentation. *J Chem Phys* 2002, **117**(24): 11320-11328.
41. Jenkins IC, Casey MT, McGinley JT, Crocker JC, Sinno T. Hydrodynamics selects the pathway for displacive transformations in DNA-linked colloidal crystallites. *P Natl Acad Sci USA* 2014, **111**(13): 4803-4808.

42. Warren BE. X-Ray Determination of the Structure of Glass (Reprint). *J Am Ceram Soc* 1992, **75**(1): 5-10.

### Figure captions:

**Figure 1. Illustration of experiment design for inducing phase transformations in DNA-NP superlattices via selective re-programming of interparticle interactions, achieved by inputting different types of strands (denoted here as blending, stapling, repelling) that modify the DNA shells of NPs in a lattice.** (a) The proto-state nanoparticles (NPs) are formed by surface tethering of  $N_p$  ( $\sim 50$ ) proto-DNA strands (see Table S1-S3 for the details of DNA designs), (b) A pair of mutually complementary base-state NPs,  $X$  and  $Y$ , are created by hybridization of proto-NP with  $N_x$  ( $\sim 34$ ) of  $x$  base-DNA strands and  $N_y$  ( $\sim 34$ ) of  $y$  base-DNA strands. (c) Assembly of the mother phase ( $MP$ ) is achieved by mixing  $X$  and  $Y$  NPs, and by post-annealing. Due to the interparticle hybridization of  $x$  and  $y$  shells from  $X$  and  $Y$  NP respectively,  $x$  and  $y$  base-DNA chains change their conformations. As result, there are  $N_{open}$  ( $\sim 8$ ) newly available sites per particle for hybridization of input strands with proto-DNAs (see supporting material). The schematics of phase transformation from  $MP$  to one of the daughter phases by the selective modification of DNA shells via re-programming DNA strands, i.e. blending ( $x&y$ ), stapling ( $s$ ), and repelling ( $r$ ). Accordingly,  $MP$  transforms into daughter phases: (d) blending ( $DP_B$ ), (e) stapling ( $DP_S$ ), and, (f) repelling ( $DP_R$ ), respectively. During these phase transformations, the particles  $X(Y)$  correspondingly hybridize with additional  $n_y/n_x$  (or  $n_x/n_y$ ),  $n_s$ , and  $n_r$  DNA strands. Note: in case of (d) blending,  $N_x$  (or  $N_y$ ) changes to  $N_x'$  (or  $N_y'$ ), e.g.,  $N_x' = N_x + n_x$ . The complementary shape pairs, shown correspondingly as dots and half circles, or triangles and squares with a triangle dent, represent the complementary DNA base pairs. The notation of subscript for particles,  $Y_x$  for instance, indicates a small portion of  $x$  strands in the shell of  $Y$  NP due to the shell modification with re-programming strands. Upon adding the strands to  $MP$ , the interparticle repulsion and attraction are changed, as depicted schematically with blue and red bars, respectively, where the bar length represents their strength.

**Figure 2. Transition from mother phase ( $MP$ ) to daughter phase ( $DP_B$ ) upon introduction of blending strands.** (a, b) The evolution of in-situ SAXS measured structure factor,  $S(q)$ , of  $MP$  at  $28^\circ\text{C}$ , after incubation with stapling strands ( $x&y$ ) at room temperature, as shown on Fig. 1. A new  $DP_B$  ( $FCC$ , indexing is shown at the top) gradually develops from  $MP$  ( $BCC$ , indexing is shown at the bottom) during an isothermal process ( $T = 28^\circ\text{C}$ ). The detailed two-phase modeling of  $S(q)$  is described in supporting materials, and the calculated  $S(q)$  are shown in Figures S8-9 and S11(a-j) for the evolution. (c) Time-dependent volume fraction ( $\phi$ ) of daughter phase ( $DP_B$ ) and nearest-neighbor center-to-center inter-particle distance ( $D_{cc}$ ), extracted from the  $S(q)$  fits, are plotted as a function of time during the transition from  $MP$  to  $DP_B$  (time counting starts when the transition is activated by bringing the system to  $T = 28^\circ\text{C}$ ). (d) The evolution of the correlation length ( $\xi$ ) and Williamson Hall slope ( $\varepsilon$ ) as a function of  $\phi$  of  $DP_B$ .

**Figure 3. Transformations induced by stapling strands.** 2D SAXS patterns and the corresponding measured (blue and red circles) and modeled (black lines) structure factors,  $S(q)$ , for systems with stapling strands from (a)  $MP$  ( $BCC$ ) transforming into (b)  $DP_{S_{HT}}$  ( $FCC$ ) at higher annealing  $T$  ( $\sim 34^\circ\text{C}$ ), while it develops into (d)  $DP_{S_{LT}}$  ( $HCP$ ) at lower annealing  $T$  ( $\sim 28^\circ\text{C}$ ). The blue arrows in  $DP_{S_{LT}}$  pattern highlight the strip features, which signify scattering from 2D crystals. (c, e) Schematics of packing for  $FCC$  ( $ABC$  periodic layered),  $HCP$  ( $AB$  periodic layered) and *quasi-2D* (weakly correlated layered) lattices. See supporting material for the details on the  $S(q)$  modeling.

**Figure 4. Morphological transition induced by repelling strands.** (a) The evolution of room-temperature measured  $S(q)$  of  $MP$  system (blue points) modified with repelling strand for different annealing temperatures,  $T$ .  $MP$  ( $BCC$ ) preserves its structure below  $34^\circ\text{C}$  (yellow points) and develops into a  $DP_R$  (*cluster*) above  $34^\circ\text{C}$  (red points). The inset in (a) illustrates the structures of the  $BCC$  and cluster phases. The modeled  $S(q)$  for the cluster state is shown in Figure S12. (b) The dependence of the correlation length,  $\xi$ , on the annealing temperature,  $T$ . The photos (insets) show a precipitated aggregate (polycrystalline) for the  $BCC$  phase, in contrast to a suspension for the cluster phase. DLS measurements (inset) show the size distribution of clusters in the suspension.

**Figure 5. The effect of input reprogramming strands on interparticle interactions, and on the consequent phase transformation pathways.** The calculation of free energy ( $F$ ) for different unit cells as a function of the DNA shell modification parameters ( $\gamma$ ), as defined in the text. (a)  $CsCl$  and  $CuAu$  for  $DP_B$  system, (b)  $CsCl$  and  $HCP/FCC$  for  $DP_S$  system, and, (c)  $CsCl$  and *cluster* morphology for  $DP_R$  system. The  $\gamma$ -dependent (as modified by re-programming strands) DNA shells are sketched, and the experimental values of  $\gamma$  are shown by blue arrows on the corresponding figures. (d) The summary of the observed strand-programmable phase transformations from mother phase  $CsCl$  to daughter phases,  $CuAu$ ,  $FCC$ ,  $HCP$ , and *cluster state*; (middle panel) the interaction model for a pair of particles.

Fig. 1

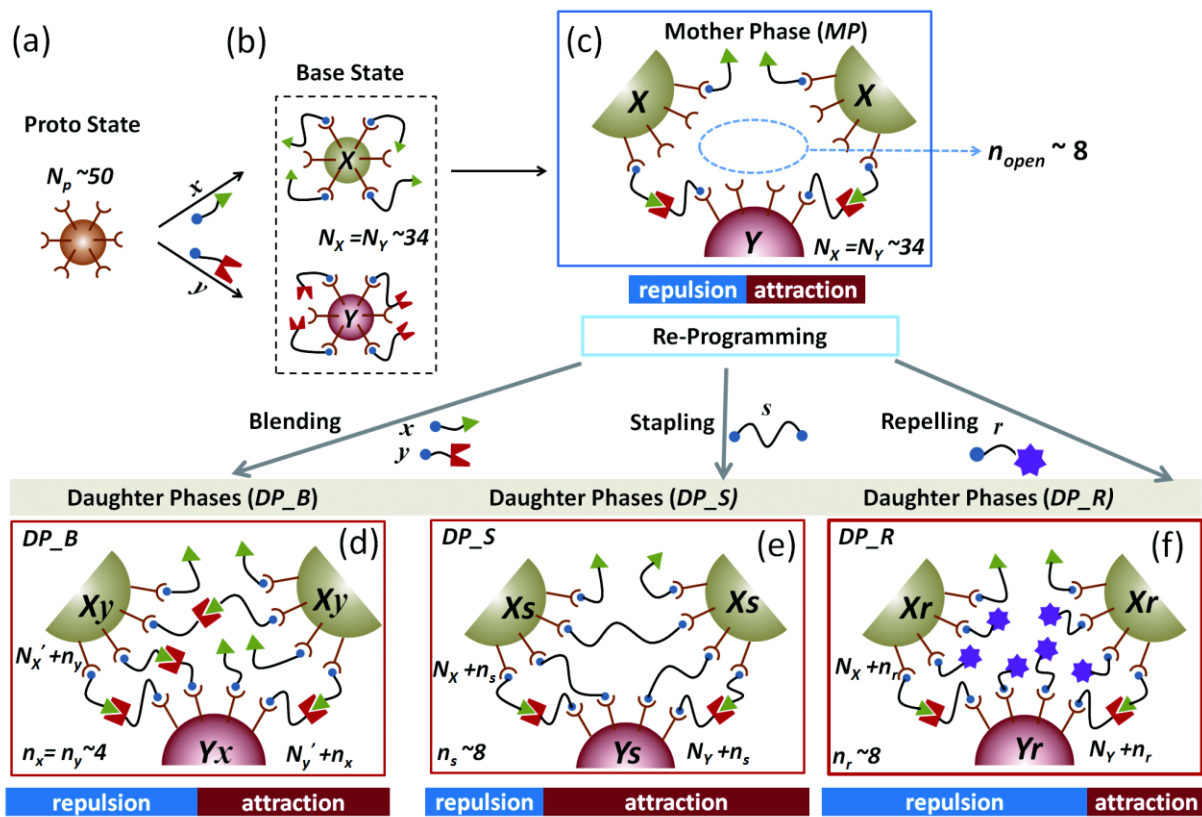


Fig. 2

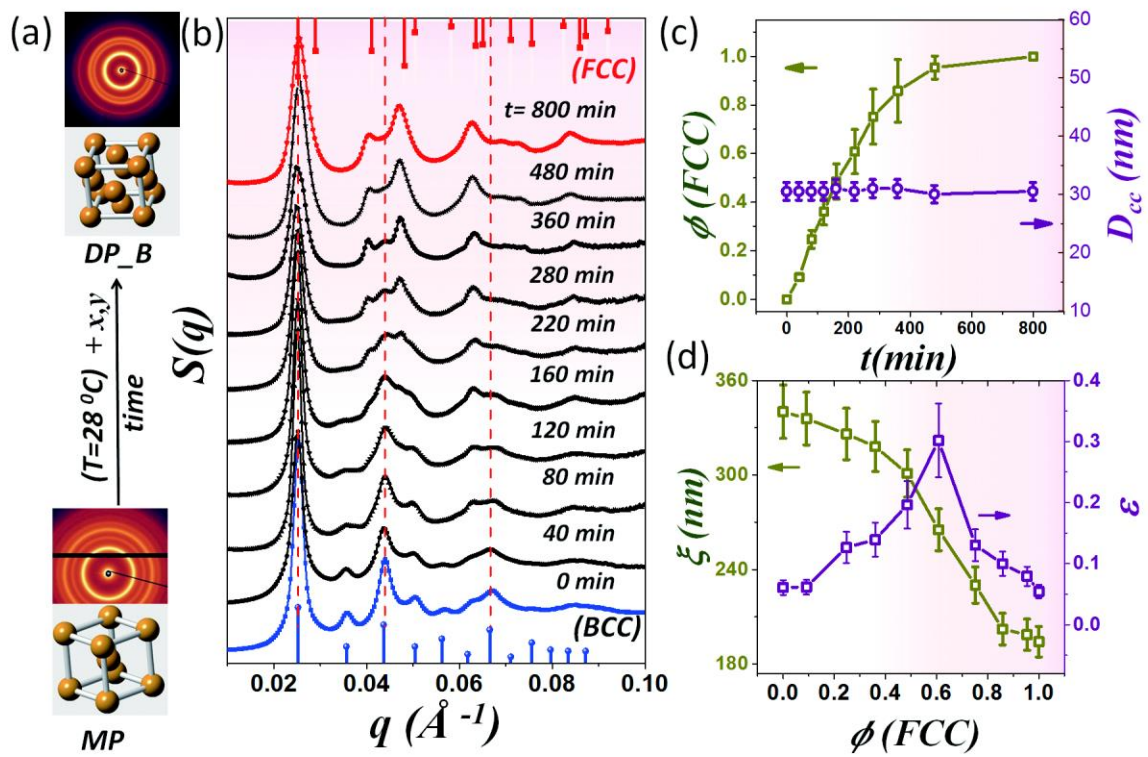


Fig. 3

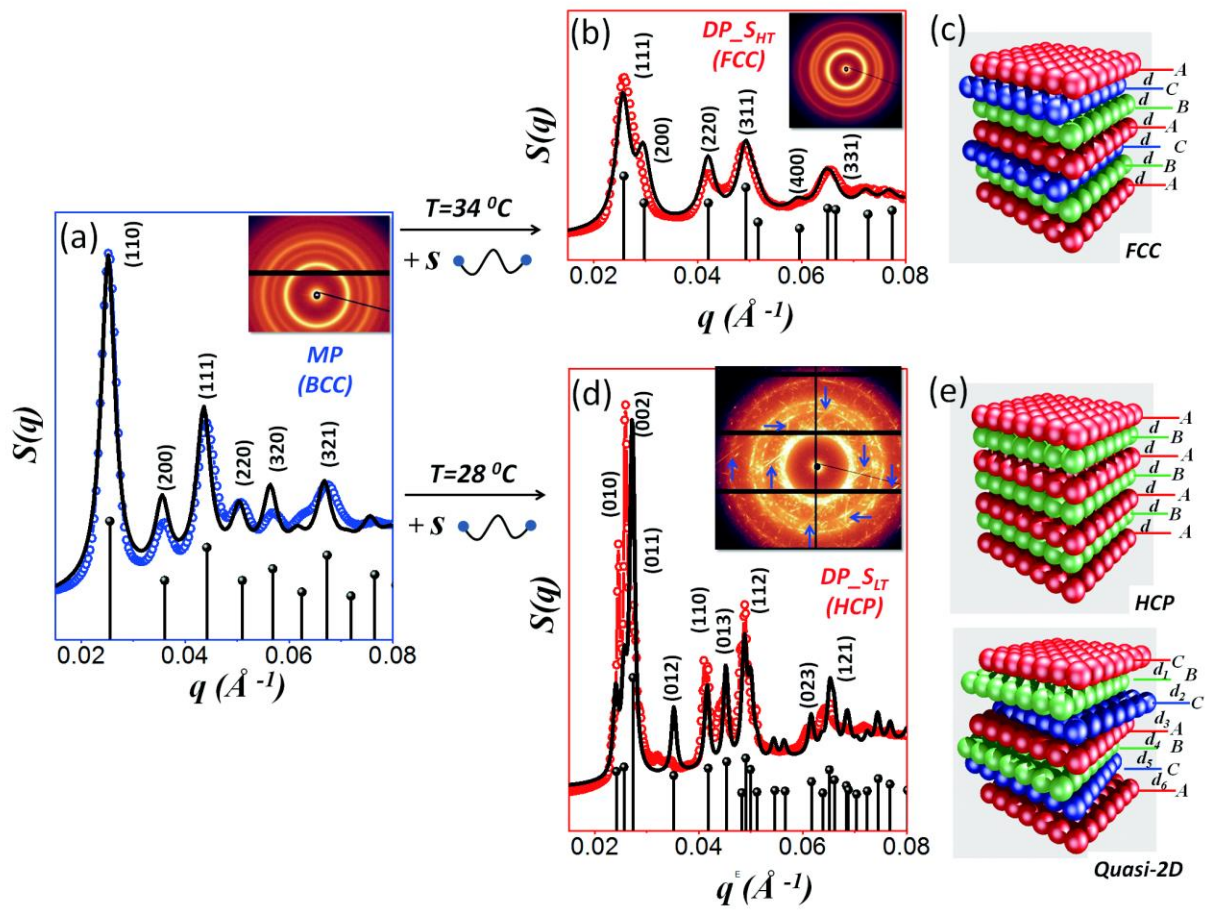


Fig. 4

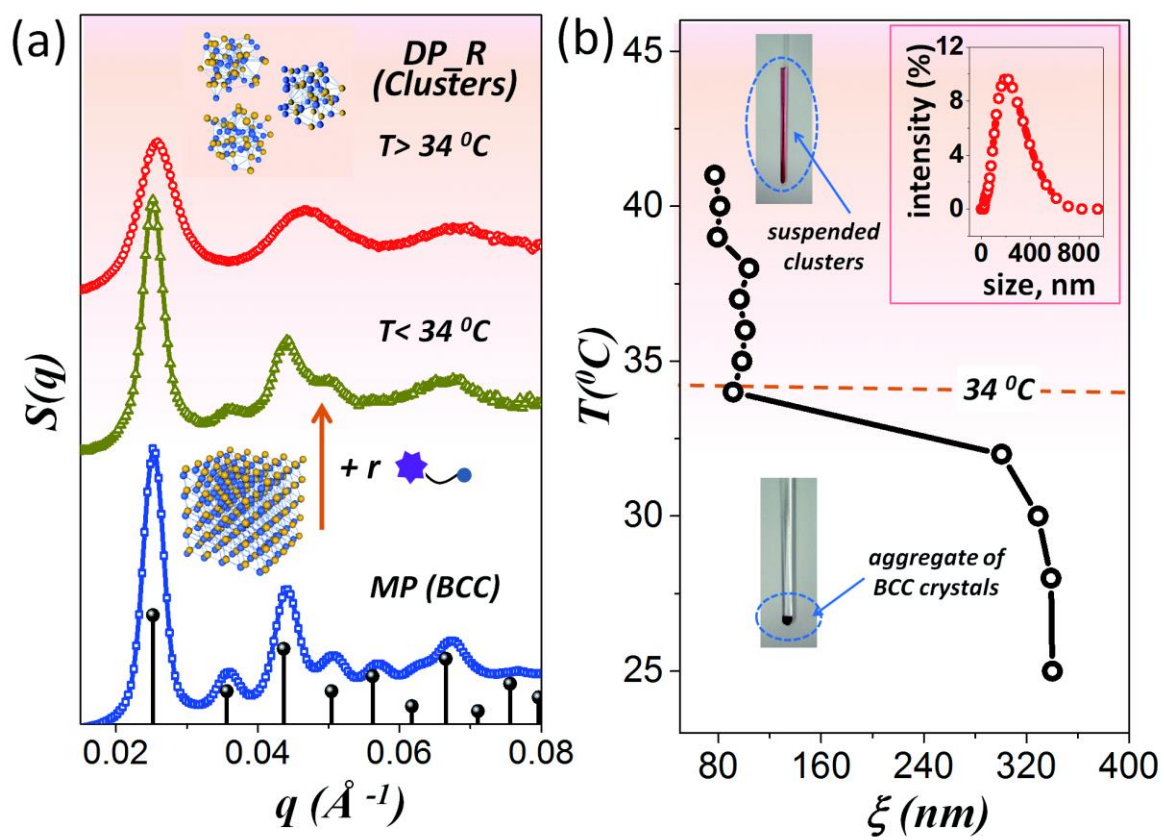


Fig. 5

